Driving reversible redox reactions at solid–liquid interfaces with the electron beam of a transmission electron microscope

Nabeel Ahmad, Guillaume Wang, Jaysen Nelayah, Christian Ricolleau, Damien Alloyeau

Driving Reversible Redox Reactions at Solid / Liquid Interfaces with the Electron Beam of a Transmission Electron Microscope

Nabeel Ahmad,[1,2] Guillaume Wang,[1] Jaysen Nelayah,[1] Christian Ricolleau,[1] and Damien Alloyeau[1,*]

1. Laboratoire Matériaux et Phénomènes Quantiques, Université Paris Diderot – CNRS, UMR 7162, Paris France

2. School of Chemical and Materials Engineering (SCME), National University of Sciences and Technology (NUST), H-12, Islamabad, Pakistan

* Corresponding Author: Damien Alloyeau, damien.alloyeau@univ-paris-diderot.fr,
Tel. +33 1 57 27 69 83, Fax. +33 1 57 27 62 41. Address. Université Paris Diderot-Paris 7, Laboratoire Matériaux et Phénomènes Quantiques, 10 rue Alice Domon et Léonie Duquet, Case courrier 7021, 75205 Paris Cedex 13, France

Key words

Liquid-cell TEM, beam effects, Cu deposition / dissolution, radiolysis, galvanic corrosion, redox reactions

Summary

Liquid-cell transmission electron microscopy (LCTEM) has opened up a new way to study chemical reactions at the interface between solids and liquids. However, understanding the effects of the electron beam in the liquid-cell has been clearly identified as one of the most important challenges to assess correctly and quantitatively LCTEM data. Here we show that the electron beam can be used to drive reversible deposition / dissolution cycles of copper shells over gold nanoparticles in methanol. Besides revealing the influence of irreversible processes on the kinetic of growth/etching cycles, this study of nanostructure behavior as a function of the dose rate highlights the possibility to switch the oxidizing or reducing nature of liquid environment only with the electron beam. The chemical and electronic processes possibly involved in these tunable redox reactions are qualitatively discussed together with their possible impacts on electrochemical LCTEM experiments.

Introduction

The redox reactions ruling the deposition or dissolution of matter at the interfaces between liquids and solids play a key role in the conception, the use and life-cycle of materials in their application media. Since the advent of liquid-cell transmission electron microscopy (LCTEM), there has been a great desire to study such growth or dissolution processes at the nanoscale, notably to provide a better understanding of nanomaterial synthesis (Liao *et al.*, 2013, Ngo & Yang, 2015), mass transport in electrochemical cells (de Jonge & Ross, 2011, Ross, 2015) and materials corrosion (Jiang *et al.*, 2014, Chee *et al.*, 2015, Elgrabli *et al.*, 2015). Nevertheless, a critical parameter in interpreting LCTEM data is to take into account the effects of the electron beam, because the strong oxidizing and reducing species that are generated by radiolysis can obviously disturb nanoscale *in situ* studies in liquid (Abellan *et al.*, 2014, Woehl & Abellan, 2016, de Jonge & Peckys, 2016). Kinetic models taking into account the volumetric production rates of radiolysis products in water, their destruction and production through chemical reactions and their diffusion, demonstrated that the steady concentrations of radicals in the irradiated area increases with the electron dose rate with power-law behaviors (Schneider *et al.*, 2014). If these theoretical considerations provide only an estimation of the power-law dependence for each radical produced in pure water, they reveal a straightforward relation between the dose rate and the concentration of radiolysis products. The two main strategies to deal with electron-beam effects in LCTEM result from this general tendency of radiolysis processes. The first practical approach consists in reducing the steady-state concentration of radiolysis products by using low dose rate to monitor dynamical phenomena that are then minimally affected by these chemical modifications. This strategy was, for instance, employed for studying the electrochemically-induced deposition and dissolution of Li on electrodes during charge/discharge cycling of battery (Holtz *et al.*, 2014, Mehdi *et al.*, 2015). The

second approach consists in exploiting radiolysis processes to drive the redox reactions leading to material transformations. Thus, the dose rate and the cumulative dose become meaningful parameters that have been successfully exploited to control and to study kinetic effects on the formation of metallic nanoparticles (Woehl *et al.*, 2012, Alloyeau *et al.*, 2015, Ahmad *et al.*, 2016). Nevertheless, it is worth noting that the reduction of metallic precursors by radiologically-produced solvated (or hydrated) electrons continuously compete with oxidative reaction that may lead to the degradation of nanomaterials. This competition between very opposite chemical pathways can be tuned by intentionally modifying solution chemistry with radical scavengers, complexing agents or by changing the solvent or its pH (Woehl & Abellan, 2016). These various methods allow driving materials behaviors by creating either reducing or oxidizing environments. However, understanding the role of the electron irradiation in this complex equilibrium remains much more complicated because of the many possible interactions between the beam and the environment and their resulting reactions (charging, modification of the pH and ionic strength, creation of highly reactive species…).

In the following, we report a simple LCTEM experiment in which the electron dose rate is used to control reversible cycles of deposition / dissolution of copper over gold nanoparticles in methanol. This study conducted with minimal modifications of the solution chemistry provides direct evidence of the electron-beam impacts on the chemical nature of the liquid environment.

Experimental

LCTEM experiments were performed using a ARM 200F microscope from JEOL (Tokyo, Japan) (Ricolleau *et al.*, 2013) equipped with a cold FEG and a commercial *in situ* sample holder (Poseidon 210) from Protochips (Morrisville, NC, USA). The accelerating voltage during all experiments was

maintained at 200 kV. The formation of the gold-copper nanostructures was realized in two steps. First experiment was performed in a methanol solution containing 1 mM of Gold (III) chloride trihydrate to grow gold nanostructures on the SiN membranes. Then, the liquid-cell was unsealed, rinsed in pure methanol, dried and reused for a second experiment with methanol containing 1 mM of Cu(II) acetylacetonate ($Cu(acac)_2$). The microfluidic system of the sample holder was also abundantly flushed with pure methanol between the two steps. For these two steps, sample preparation was done by depositing a 2.4 µl droplet of Au or Cu precursors in methanol on the small E-chip. The large E-chip was placed on top with the SiN membranes windows in cross configuration to reduce bowing effects towards the microscope vacuum. The entire assembly was made vacuum tight by using O-rings and then closing the sample holder lid over the liquid cell assembly by means of brass screws (figure S1). Low-magnification imaging was used to confirm that the liquid cell was always fully-filled with liquid. The Au spacers between E-chips were 150 nm thick and the experiments were performed in the corners of observation window, where liquid thickness is minimum. A 5 µL/min flow of methanol containing 1 mM of Au precursors (first step) or 1 mM of Cu precursors (second step) was continuously injected in the liquid-cell. LCTEM imaging was performed in scanning mode on a High Angular Annular Dark Field detector (STEM – HAADF) with a pixel dwell time of 5 µs. For the growth of gold nanoparticles, small probe size (8C) and small condenser aperture (50 µm in diameter) were used to reduce the beam current to 1.5 pA. For the growth of copper on gold nanoparticles the beam current was increased up to 8.4 pA by using a larger probe size (5C). In STEM mode, dividing the beam current by the imaged area and the electron charge allows calculating the electron dose rate in units of electrons/$Å^2$s. This crucial parameter for radiolysis processes was modulated in our experiment by changing the magnification. STEM imaging was mostly performed on the top E-chip (the small one in the JEOL ARM microscope) to improve image resolution and quality.

Results and discussion

As a first step, a low-dose LCTEM experiment was conducted to form gold nanoparticles on the SiN membranes of the liquid-cell (Fig 1a). Chloroauric acid diluted in methanol was imaged in STEM-HAADF mode with dose rate ranging from $4.1*10^{-3}$ to $3.7*10^{-2}$ electrons/$Å^2$s (magnification from 50k to 150k). The main primary products of methanol radiolysis are solvated electrons (e_s) and $CH_3OH^{\bullet}$ radicals. (Baxendale & Wardman, 1975, Ferradini & Jay-Gerin, 1996) These strong reducing and oxidizing species are equivalent to the aqueous electrons (e_h) and the hydroxyl radicals ($OH^{\bullet}$) formed during the radiolysis of water, respectively. Solvated electrons most likely reduce gold precursors leading to the nucleation and growth of Au nanoparticles. As in water, the electron dose rate allows controlling the growth kinetic of the nanoparticles indicating that the steady-state concentration of solvated electrons (and probably other radiolysis products) increases with the dose rate (Fig. 1b). As previously reported (Alloyeau et al., 2015), low-dose conditions induce the formation of 2D platelets with triangular and hexagonal forms, together with 3D facetted nanoparticles with much brighter contrast on the STEM-HAADF images because of their higher thickness (Fig. 1a). The percentage of 2D and 3D nanoparticles are equivalent in methanol and in water (Fig. S2).

After forming several patches of Au nanoparticles on the SiN membranes, the liquid cell was unsealed, rinsed with methanol and dried to make sure it was clean from gold precursors for the second step of the experiments. The same liquid-cell was sealed again and LCTEM experiment was carried out to form Cu shells over the Au nanoparticles remaining on the SiN membranes. Cu(II) acetylacetonate diluted in methanol was imaged in STEM HAADF mode with dose rate ranging from $3.8 *10^{-3}$ to 9.5 electrons/$Å^2$s (magnification from 20k to 1000k). As in a first step, the metallic complexes are most likely reduced by solvated electrons (and probably by $H^{\bullet}$ also

produced by radiolysis of methanol). In all the areas studied, Cu-layer growth systematically starts for dose rate above 6.1 electrons/Å^{2}s (magnification of 800k). Interestingly, Cu deposition only occurs on the gold nanoparticles and not on the SiN membranes (Fig. 2a). This localized growth mechanisms could be explained by a higher chemical affinity of Cu monomers for capping-agent-free gold surfaces than for amorphous SiN or by a catalytic effect of the gold surfaces since the reduction potential of metal ions can be increased upon adsorption on nanoparticles (Sakamoto *et al.*, 2007). Interestingly, Hu et al. theoretically demonstrate that Cu(acac)2 can chemisorbs on metal surfaces and decomposes easily into a Cu atom and acac-ligands *via* a sequential dissociation and reduction of the Cu ion (Hu *et al.*, 2015). It has been also proposed that the many secondary electron generated by irradiated metallic interfaces can locally increase the energy absorbed by the solvent (Schneider, 2016). The resulting enhancement of radiolytic Cu growth would then be confined at the vicinity of the Au nanoparticles, because of the short mean free path of secondary electrons. Cu deposition follows a Volmer-Weber growth mode (Venables *et al.*, 1984), consisting in the nucleation of small 3D clusters on the Au surfaces that rapidly grow and coalesce to form rough layers over all the 2D or 3D gold nanoparticles present in the irradiated area. Full covering of the Au surface with 50 nm thick Cu layers was obtained in less than a minute. Surprisingly, as soon as the electron dose rate was reduced down to 1.5 electrons/Å^{2}s (magnification 400k), the rapid dissolution of these Cu films was observed (fig. 2b). More importantly, these growth/etching phenomena are cyclic processes that can be repeated many times on the same area with the same dose-rate-dependant behaviour. By cycling back and forth between deposition and dissolution, we could clearly establish that Cu growth is activated for dose rate greater than or equal to 6.1 electrons/Å^{2}s (magnification of 800k), while Cu dissolution occurs for dose rate below or equal to 1.5 electrons/Å^{2}s (magnification 400k). At intermediate magnifications between these two ranges

neither growth nor etching is possible. As observed in figure 3, the Cu shells formed when magnification reaches 800k are stable when magnification is maintained at 600k or 500k.

Repeating growth and etching cycles on the same nanostructure reveals further interesting dynamics. Indeed, if the dose-rate-dependent behaviour of Cu remains similar over several cycles, the repetition of these reversible processes clearly affect the growth kinetic and the resulting structure of the Cu layer. The Figure 4 shows Au-Cu nanostructures after four consecutive Cu-growth steps of 20 seconds performed at 800k (Fig. 4b, 4d, 4f and 4h) and three dissolution steps of several minutes performed at 400k (Fig. 4c, 4e and 4g). The thickness of the Cu-shells obtained after 20 seconds of growth obviously increases with cycling, owing to the rising of the growth rate from a cycle to another (figure 5). Additionally, surface roughness also increases with cycling. This tendency of Cu layers to be more and more dendritic when getting thicker highlights that the growth processes are increasingly limited by the diffusion of Cu atom from the solution to the Au/Cu nanoparticles (Ahmad et al., 2016). Figure 4 also reveals that deposition/dissolution cycles are not fully reversible. Indeed, Cu layers are never completely dissolve at the end of dissolution steps and many residual Cu particles are still observed on the Au nanoparticles after several minutes of observation at 400k. Some of these persistent deposits do not seems anymore attached to the gold surface. We note that these Cu residues still persist even if we drastically reduce the magnification. Interestingly, the amount of Cu residues rises with cycling. This irreversible phenomenon certainly contributes to the growth-process enhancement of the Cu layers as these persistent Cu nanoparticles act as pre-existing nucleation sites during the next layer formation. The Cu deposition/dissolution mechanisms, here controlled by the electron beam, bear striking resemblance to electrochemical processes that occurs at the electrode/electrolyte interface during charge/discharge cycling of batteries. Mehdi et al. have notably shown that Lithium deposition/dissolution mechanisms on a Pt

working electrode were similarly influenced by the presence of remnant Li on the Pt surface after the discharge of their operando electrochemical cell (Mehdi et al., 2015).

Radiolysis modelling developed by Schneider and co-workers indicated that the concentration ratio of the primary reducing (e_h) and oxidizing ($OH^{\bullet}$) species produced in pure water slightly increases with the dose rate (Schneider et al., 2014). This qualitative result was exploited to explain the beam-induced growth and dissolution of gold nanoparticles observed in water by the same authors. As in our LCTEM experiment in methanol, nanoparticle growth was activated at higher dose rate than their dissolution and a dose-rate range of stability was observed in between. By drawing an analogy with water, we can then hypothesize that in methanol high dose rate generates a reducing environment because of predominant effects of solvated electrons, whereas low dose rate induces an oxidizing medium due to a higher concentration of $CH_3OH^{\bullet}$. In between, the dose-rate range of Cu-shell stability certainly corresponds to an equilibrium between competing redox reactions. Although this hypothesis satisfactorily explains the beam-dependent behavior of metals, many phenomena can also impact the redox reactions driving growth and dissolution processes. First of all, the only presence of $Cu(acac)_2$ influences the radiation chemistry of methanol because it inevitably leads to additional reactions, including the reduction of this metal precursor, that modify the steady state concentrations of radiolysis products (Park *et al.*, 2015). In the experiment of Schneider *et al*. the presence of CTAB made possible the dissolution of Au nanoparticles *via* oxidative reactions with $OH^{\bullet}$, because halide ions, like Br^-, are complexing agents that lower the reduction potential of metals (Jiang et al., 2014, Schneider et al., 2014). In our experiments, such complexification mechanisms can be rule out because the solution only contains Cu precursors. However, the direct contact between Au and Cu in an electrolytes solution can lead to the galvanic corrosion of Cu. Indeed, the difference in voltage potential between the Au and Cu (Roberge, 1999)

will favor the dissolution of Cu that acts as the anode in a galvanic cell. In a similar way that dead Li is formed during Li-battery cycling, the residual copper observed after the dissolution steps could then results from local contact losses between the Au cores and the Cu shells, preventing galvanic corrosion processes. Furthermore, the stability of metals in solution is directly linked to their voltage potential and the pH of the solution. On the one hand, the pH of the reaction medium is expected to change under irradiation (Schneider et al., 2014), but local pH measurements remain challenging. On the other hand, the electric potential of metals can be modify by charging effects within the SiN substrate that increase with the dose rate and could generate charge transfer between the amorphous film and the supported nanoparticles (Woehl & Prozorov, 2015). Evaluating the respective weight of all these parameters is a key milestone to provide a quantitative understanding of the stability of metallic nanoparticles in LCTEM experiments.

Finally, we want to discuss the possible implications of these results for LCTEM investigations, notably for electrochemical studies that have been one of the primary motivation for the development of this technique (Williamson *et al.*, 2003). Common practice for studying electrochemical interfacial reactions consists in maintaining the electron dose below the electrolyte damage threshold. (Abellan et al., 2014, Holtz et al., 2014, Mehdi et al., 2015). Nevertheless, if the threshold of visible phenomena such as metal growth or polymerization, can be calibrated with LCTEM imaging, other chemical modifications can affect the electrochemical reactivity of materials without necessarily changing the electrolyte contrast. The present works show that very low-dose rate (< 1 electrons/$Å^2$s) in methanol seems to favour oxidizing environment that could affect externally-controlled deposition and dissolution of metals. It is worth noting that comparing cyclic voltammetry experiments acquired in a liquid-cell with and without electron irradiation

could be an interesting approach to quantify the chemical and/or electronic modifications of the environment as a function of the dose rate.

Conclusion

We have shown that the electron beam of a TEM can be exploited to control deposition / dissolution cycles of Cu nanoshells over Au nanoparticles in methanol. The mechanistic study of growth/etching cycles of Cu layers reveals that the kinetic of formation of Cu nanoshells increases with cycling because of the incomplete dissolution of the previous layers. The similar dose-rate-dependent behaviors of metallic nanostructures observed in aqueous and organic solvents allows assuming that the oxidizing or reducing nature of many environments can be tuned with the electron beam. In the present case, high dose rates create reducing media leading to the growth of metallic nanostructures, whereas low dose rates reinforce oxidizing media favoring metal etching. The dissolution of metallic nanostructures is not observed in all LCTEM experiments because metal etching most likely requires the help of complexing agents or bimetallic corrosion processes. More generally, this work highlights the crucial need for a better understanding of the electron beam effects that are neither linear with the dose rate nor necessarily marginal when very low-dose rate are used.

Acknowledgements

The authors gratefully acknowledge stimulating discussions with Dr. Frances Ross and Dr. Nicholas Schneider on the data. We also acknowledge the financial support of the Region Ile-de-

France (convention SESAME E1845 for the JEOL ARM 200F electron microscope installed at the Paris Diderot University), the Labex SEAM (Plas-Mag project), the CNRS (Defi-Nano Program) and National University of Sciences and Technology (NUST) for supporting the PhD grant of Nabeel Ahmad.

Figures

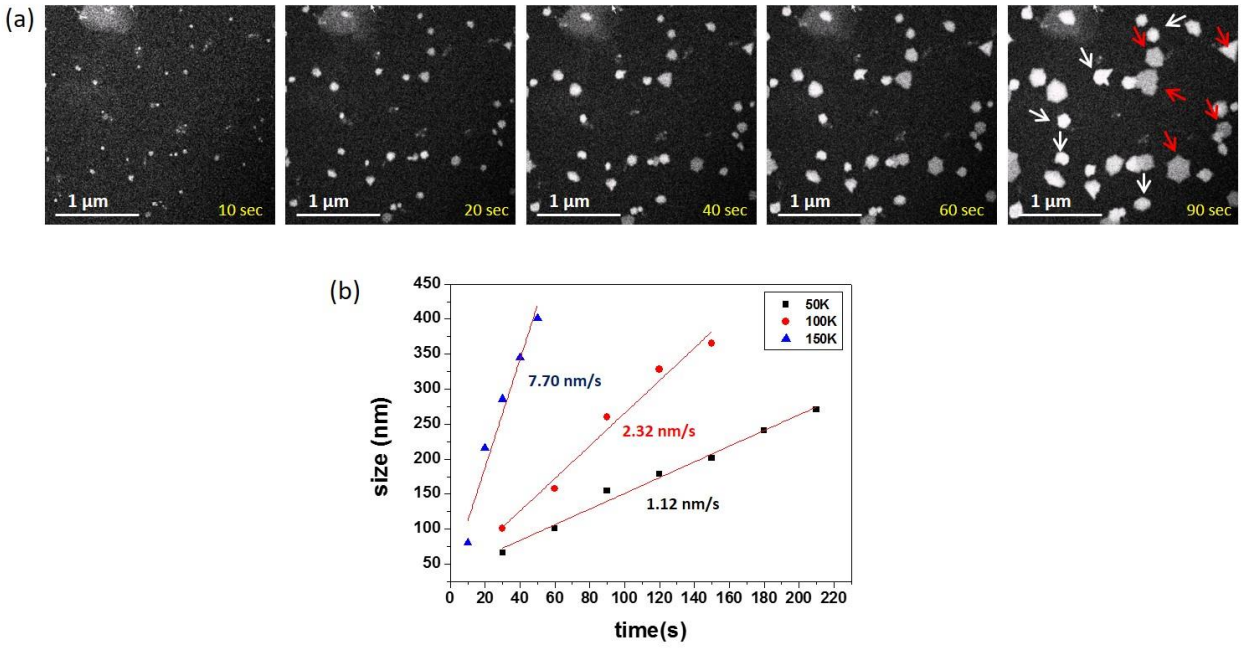

Figure 1. Growth of gold nanoparticles by radiolysis in methanol. (a) Au nanoparticles growth monitored by STEM HAADF with a magnification of 80 k (dose rate = 10^{-2} electrons/Å^{2}s). Some 3D and 2D nanoparticles are indicated by white and red arrows, respectively. The irradiation time is indicated in the bottom right corner of each image. (b) Mean size of 2D plates as a function of time for different magnification indicated in the right top inset (dose rate is proportional to the square of magnification). The mean growth rate is indicated below each linear fit.

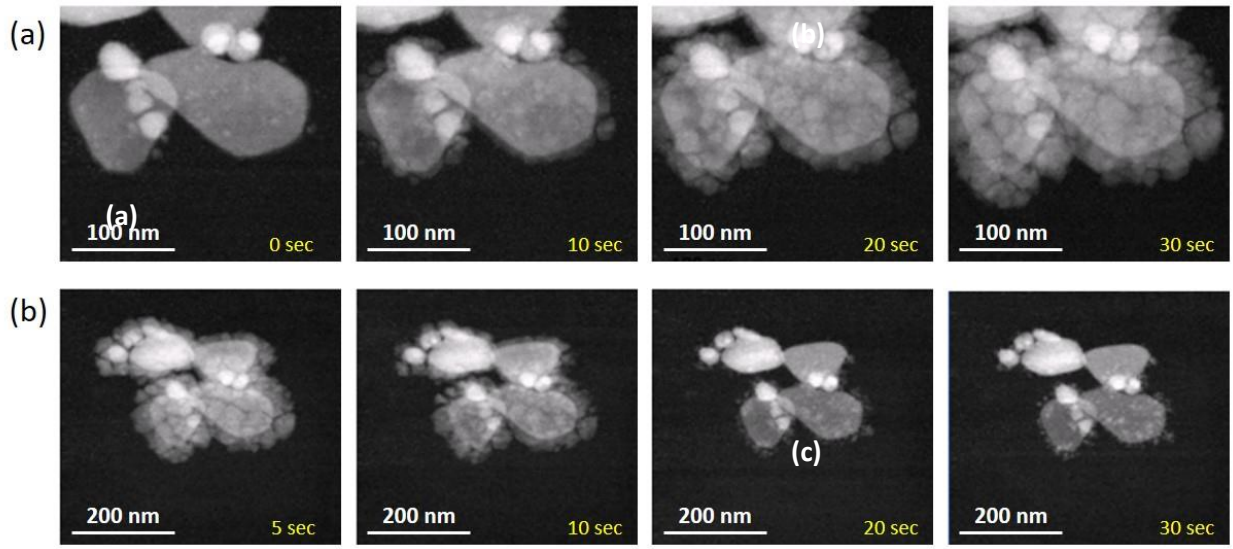

Figure 2. Cycle of deposition and dissolution of Cu nanoshell on gold nanoparticles in methanol. (a) Nucleation and growth of Cu nanoshells monitored by STEM HAADF with a magnification of 800 k (dose rate = 6.1 electrons/Å^{2}s). (b) Dissolution of Cu nanoshells monitored by STEM HAADF with a magnification of 400 k (dose rate = 1.5 electrons/Å^{2}s). The irradiation time at a given magnification is indicated in the bottom right corner of each image.

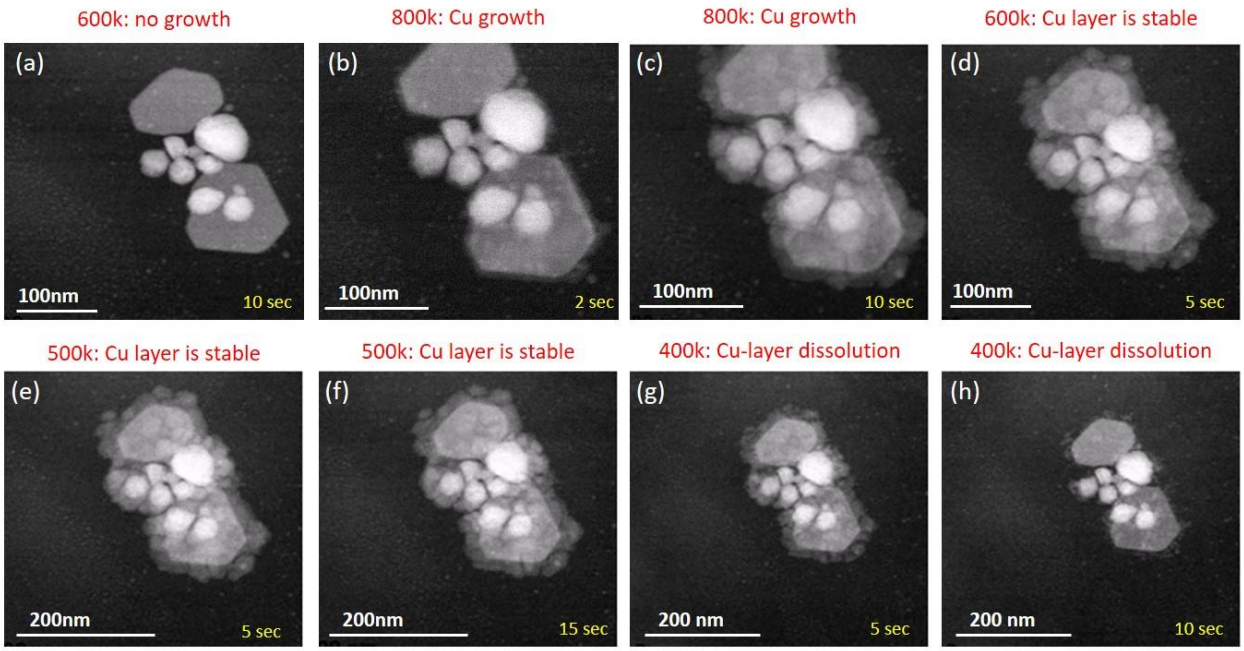

Figure 3. Strutural stability of the nanoparticles at intermediate dose rate. (a – h) Cycle of deposition and dissolution of Cu nanoshell on gold nanoparticles in methanol. The magnification and the observed phenomena are indicated above each image. The irradiation time at a given magnification is indicated in the bottom right corner of each image. At 500k and 600k, Cu shells are either absente (image a) or stable (images e and f).

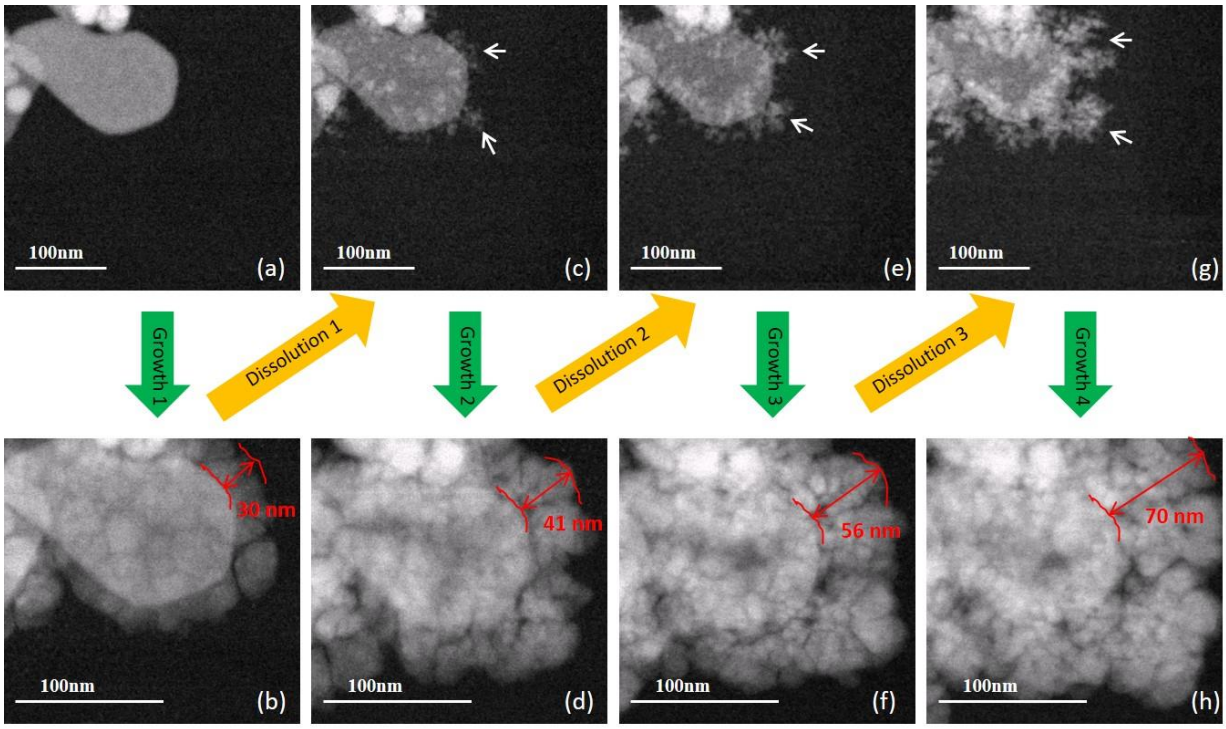

Figure 4: Four consecutive deposition/dissolution cycles of Cu nanoshells on gold nanoparticles in methanol. (a) Gold nanoparticles before Cu shell growth. (b, d, f, h) STEM-HAADF images of Au-Cu nanostructures after four consecutive Cu-growth steps of 20 seconds performed at 800k (dose rate = 6.1 electrons/Å^{2}s). The thickness of the Cu layers is indicated on each image. (c, e, g) STEM-HAADF images of Au-Cu nanostructures after three consecutive dissolution steps of several minutes performed at 400k (dose rate = 1.5 electrons/Å^{2}s). The remnant Cu on the gold nanoparticles after the dissolution steps is indicated by white arrows.

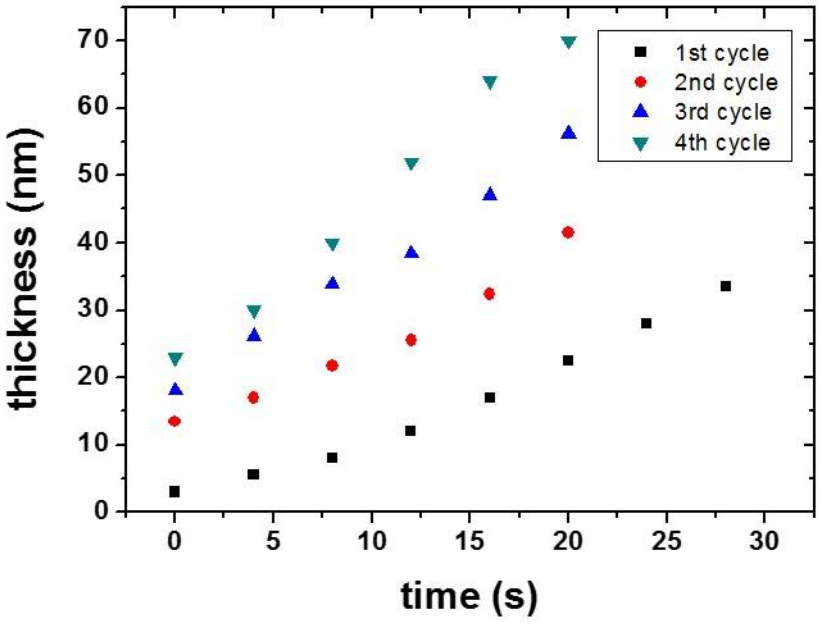

Figure 5: Evolution of the growth rate during deposition/dissolution cycling. Thickness of the Cu layer seen in figure 3 as a function of time during four consecutive growth steps.

References:

Abellan, P., Mehdi, B. L., Parent, L. R., Gu, M., Park, C., Xu, W., Zhang, Y., Arslan, I., Zhang, J.-G., Wang, C.-M., Evans, J. E. & Browning, N. D. (2014) Probing the Degradation Mechanisms in Electrolyte Solutions for Li-Ion Batteries by in Situ Transmission Electron Microscopy. *Nano Letters,* **14,** 1293-1299.

Ahmad, N., Le Bouar, Y., Ricolleau, C. & Alloyeau, D. (2016) Growth of dendritic nanostructures by liquid-cell transmission electron microscopy: a reflection of the electron-irradiation history. *Advanced Structural and Chemical Imaging,* **2,** 9.

Alloyeau, D., Dachraoui, W., Javed, Y., Belkahla, H., Wang, G., Lecoq, H., Ammar, S., Ersen, O., Wisnet, A., Gazeau, F. & Ricolleau, C. (2015) Unravelling Kinetic and Thermodynamic Effects on the Growth of Gold Nanoplates by Liquid Transmission Electron Microscopy. *Nano Letters,* **15,** 2574-2581.

Baxendale, J. H. & Wardman, P. (1975) *The Radiolysis of Methanol: Product Yields, Rate Constants, and Spectroscopic Parameters of Intermediates,* National Bureau of Standards.

Chee, S. W., Pratt, S. H., Hattar, K., Duquette, D., Ross, F. M. & Hull, R. (2015) Studying localized corrosion using liquid cell transmission electron microscopy. *Chemical Communications,* **51,** 168-171.

de Jonge, N. & Peckys, D. (2016) Live Cell Electron Microscopy Is Probably Impossible. *ACS Nano,* **10,** 9061.

de Jonge, N. & Ross, F. M. (2011) Electron microscopy of specimens in liquid. *Nat. Nanotechnol.,* **6**.

Elgrabli, D., Dachraoui, W., Menard-Moyon, C., Liu, X. J., Begin, D., Begin-Colin, S., Bianco, A., Gazeau, F. & Alloyeau, D. (2015) Carbon nanotube degradation in macrophages: live nanoscale monitoring and understanding of biological pathway. *ACS. Nano.,* **9**.

Ferradini, C. & Jay-Gerin, J. P. (1996) Quelques aspects actuels de la radiolyse du méthanol liquide: Une revue. *Radiation Physics and Chemistry,* **48,** 473-480.

Holtz, M. E., Yu, Y. C., Gunceler, D., Gao, J., Sundararaman, R., Schwarz, K. A., Arias, T. A., Abruna, H. D. & Muller, D. A. (2014) Nanoscale imaging of lithium ion distribution during in situ operation of battery electrode and electrolyte. *Nano. Lett.,* **14**.

Hu, X., Schuster, J., Schulz, S. E. & Gessner, T. (2015) Surface chemistry of copper metal and copper oxide atomic layer deposition from copper (ii) acetylacetonate: a combined first-principles and reactive molecular dynamics study. *Physical Chemistry Chemical Physics,* **17,** 26892-26902.

Jiang, Y., Zhu, G., Lin, F., Zhang, H., Jin, C., Yuan, J., Yang, D. & Zhang, Z. (2014) In situ Study of Oxidative Etching of Palladium Nanocrystals by Liquid Cell Electron Microscopy. *Nano Letters,* **14,** 3761-3765.

Liao, H. G., Niu, K. Y. & Zheng, H. M. (2013) Observation of growth of metal nanoparticles. *Chem. Commun.,* **49**.

Mehdi, B. L., Qian, J., Nasybulin, E., Park, C., Welch, D. A., Faller, R., Mehta, H., Henderson, W. A., Xu, W., Wang, C. M., Evans, J. E., Liu, J., Zhang, J. G., Mueller, K. T. & Browning, N. D. (2015) observation and quantification of nanoscale processes in lithium batteries by operando electrochemical (S)Tem. *Nano. Lett.,* **15**.

Ngo, T. & Yang, H. (2015) Toward ending the guessing game: study of the formation of nanostructures using in situ liquid transmission electron microscopy. *J. Phys. Chem. Lett.,* **6**.

Park, J. H., Schneider, N. M., Grogan, J. M., Reuter, M. C., Bau, H. H., Kodambaka, S. & Ross, F. M. (2015) Control of electron beam-induced au nanocrystal growth kinetics through solution chemistry. *Nano. Lett.,* **15**.

Ricolleau, C., Nelayah, J., Oikawa, T., Kohno, Y., Braidy, N., Wang, G., Hue, F., Florea, I., Bohnes, V. P. & Alloyeau, D. (2013) Performances of an 80 - 200 kV microscope employing a cold-FEG and an aberration-corrected objective lens. *Microscopy.,* **62**.

Roberge, P. (1999) *Handbook of Corrosion Engineering,* McGraw-Hill Professional.

Ross, F. M. (2015) Opportunities and challenges in liquid cell electron microscopy. *Science,* **350**.

Sakamoto, M., Tachikawa, T., Fujitsuka, M. & Majima, T. (2007) Photochemical Formation of Au/Cu Bimetallic Nanoparticles with Different Shapes and Sizes in a Poly(vinyl alcohol) Film. *Advanced Functional Materials,* **17,** 857-862.

Schneider, N. (2016) Electron Beam Effects in Liquid Cell TEM and STEM. In: *Liquid Cell Electron Microscopy* (ed. F. Ross). Cambridge: Cambridge University Press.

Schneider, N. M., Norton, M. M., Mendel, B. J., Grogan, J. M., Ross, F. M. & Bau, H. H. (2014) Electron-water interactions and implications for liquid cell electron microscopy. *J. Phys. Chem. C,* **118**.

Venables, J. A., Spiller, G. D. T. & Hanbucken, M. (1984) Nucleation and growth of thin films. *Reports on Progress in Physics,* **47,** 399.

Williamson, M. J., Tromp, R. M., Vereecken, P. M., Hull, R. & Ross, F. M. (2003) Dynamic microscopy of nanoscale cluster growth at the solid-liquid interface. *Nat. Mater.,* **2**.

Woehl, T. J. & Abellan, P. (2016) Defining the radiation chemistry during liquid cell electron microscopy to enable visualization of nanomaterial growth and degradation dynamics. *Journal of Microscopy***,** n/a-n/a.

Woehl, T. J., Evans, J. E., Arslan, I., Ristenpart, W. D. & Browning, N. D. (2012) Direct in situ determination of the mechanisms controlling nanoparticle nucleation and growth. *ACS. Nano.,* **6**.

Woehl, T. J. & Prozorov, T. (2015) The Mechanisms for Nanoparticle Surface Diffusion and Chain Self-Assembly Determined from Real-Time Nanoscale Kinetics in Liquid. *The Journal of Physical Chemistry C,* **119,** 21261-21269.